

Benefits of a single photon wavefront sensor

T.Y. Chew¹ and R.G. Lane²

¹University of Canterbury, Dept. Electrical & Electronic Engineering

²Applied Research Associates, New Zealand

Email: tyc20@student.canterbury.ac.nz

Abstract

Adaptive optics systems are used to cancel the effects of atmospheric turbulence on the image quality of astronomical telescopes. These systems require wavefront sensors to detect the effects of atmospheric turbulence, deformable mirrors to cancel the turbulence effects, and control computers to coordinate their control loops. We investigate wavefront sensors that operate on individual photon measurements to estimate the effects of atmospheric turbulence. This can potentially improve the performance of an adaptive optics system by reducing the delay lag time in the control loop. Simulations of a pyramid wavefront sensor are used to show the benefits of updating the wavefront estimate with the arrival of each individual photon.

Keywords: Adaptive optics, pyramid wavefront sensor, photon counting

1 Introduction

Astronomical observations depend on telescopes to collect the information carried by light from distant objects. However, ground based astronomical telescopes are severely limited in resolution due to atmospheric turbulence, which creates random time varying optical aberrations. Today, the effects of atmospheric turbulence can be rapidly corrected using adaptive optics systems. Wavefront aberrations caused by the turbulent atmosphere are measured with a wavefront sensor, and corrected with a deformable mirror using computer control.

Most wavefront sensors do not measure the wavefront aberrations directly. Instead, information on the aberrations caused by the atmosphere is obtained from observations of photons from a bright point-like object. Wavefront sensors work by accumulating large numbers of photons with CCD sensors, treating their intensity distribution in aggregate as an image. The CCD detector elements need to be exposed over a period of time in order to build up the light levels to overcome detector read noise. Unfortunately, as the atmosphere is continually changing, this finite integration time introduces modelling errors. We examine the performance improvements that can be obtained from using single photon counting devices in the wavefront sensors of adaptive optics systems.

2 Adaptive optics control systems

The feedback control used in an adaptive optics system is shown simplified in figure 1. Light

from a guide star is collected by the telescope primary mirror, and contains aberrations caused by atmospheric turbulence. The continually changing wavefront is corrected with a deformable mirror in the light path. Due to imperfect correction, the reduced errors in the residual wavefront continue to degrade the image quality in the main imaging channel. Some light from the guide star is diverted, providing information on the residual wavefront, to the wavefront sensor. The estimate of the residual wavefront is used to update the mirror actuation signals, closing the control loop. The deformable mirror thus represents an estimate of the incoming wavefront aberrations at any instance in time.

The performance of the system is limited by delays in the control loop, the light levels available and the specifications of the wavefront sensor and deformable mirror.

1. The loop delay arises from the CCD integration time, processing delay of the control computer, and lag in the response time of the deformable mirror. The response time of deformable mirrors is typically less than or around 1 millisecond.

2. The light level determines the ultimate performance of the wavefront sensor. Aside from integration time constraints, it is also limited by the availability of bright natural guide stars. This is a measure of the sky coverage provided by the adaptive optics system.

3. The deformable mirror is limited to correcting a finite number of wavefront modes because of

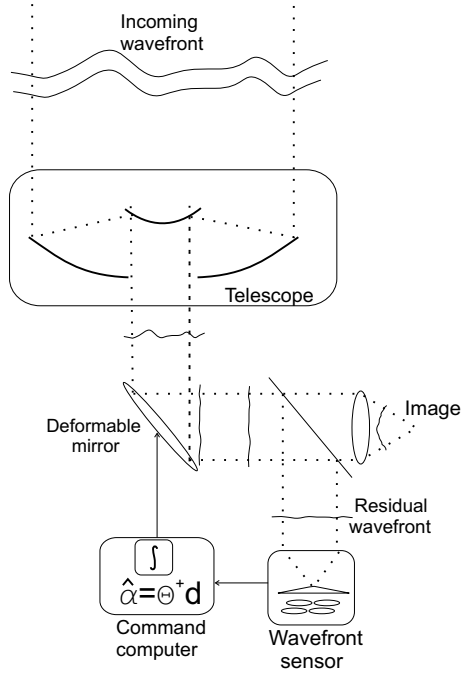


Figure 1: Simplified layout of an adaptive optics system, with closed-loop control.

the limited number of actuators driving the mirror faceplate.

The CCD integration time is constrained by three different factors - the read noise in the CCD, the signal level, and the atmospheric time constant [1], which quantifies the rate of change in the input wavefront. Read noise is roughly inversely proportional to the exposure time, while the signal level, measured here using the photon count, is directly proportional to the exposure time. The atmospheric time constant is generally in the order of several milliseconds, placing a limit on the maximum CCD exposure time.

The speed of the control computer is limited by wavefront estimation calculations, which typically involve a matrix multiplication. This is of the order of $O(nm)$ for n sensor measurements and m mirror actuator signals. For example, as detailed in later sections, our simulation uses 64×64 sampling of the aperture, and estimates $m = 20$ wavefront modes. The aperture sampling results in about $n = 4000$ slope measurements. To complete 80000 calculations in 1ms would require an 80MHz processor.

3 Wavefront sensor model

The concept behind the single photon wavefront sensor can be applied to any linear wavefront sensor. This paper focuses on the pyramid wavefront sensor [2].

The pyramid wavefront sensor, shown in figure 2, consists of a pyramidal prism placed at the focal

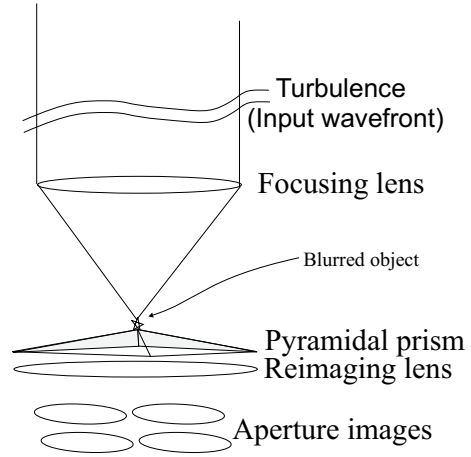


Figure 2: Layout of a pyramid wavefront sensor.

plane. The focal plane of the telescope is subdivided and each quadrant is re-imaged separately, forming 4 images of the aperture (figure 3).

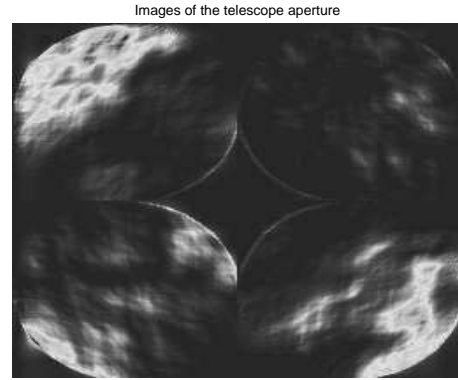


Figure 3: Images of the aperture formed through each quadrant at the sub-divided focal plane. The images can be combined to form a signal proportional to the wavefront slope.

By combining the intensity distribution at the same point in each aperture image, a signal that is linear with respect to the wavefront slope at that point can be formed. In this paper, we chose to use a modal estimation method to simulate the wavefront estimation process. The wavefront aberration $W(x, y)$ is represented as linear combinations of basis functions or modes

$$W(x, y) = \sum_i \alpha_i Z_i(x, y) \quad (1)$$

where (x, y) represent spatial coordinates of the wavefront.

The basis functions $Z_i(x, y)$ used in this paper are the Zernike polynomials [3], which are orthogonal over a circle of radius 1, centred on the origin. The coefficients of the modes, α , fully describes the wavefront. The signal from the pyramid wavefront

sensor, being linearly dependent on the wavefront slope, is represented with a matrix operation.

$$d = \Theta\alpha \quad (2)$$

where d is the signal from the wavefront sensor, α is the Zernike modal coefficients describing the wavefront, and Θ the interaction matrix between the wavefront and sensor signal.

3.1 Photon counting wavefront sensor

The linearity of the sensor image to the wavefront allows us to estimate the wavefront photon by photon. An example of a typical image frame with just one photon is shown in figure 4.

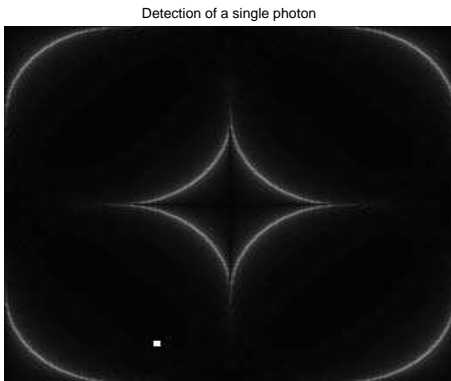


Figure 4: The arrival of a single photon at the pyramid sensor detector, shown superimposed against an outline of the aperture image.

Assuming perfect photon counting devices are used, we propose to study the benefits from their use in adaptive optics systems. The primary benefit arises from the reduce CCD integration time requirements. Instead of updating the deformable after integrating the photons over a fixed period of time, the mirror can be updated after the arrival of each individual photon. A further improvement is that it is also possible to reduce the calculation time since the effect of a single photon arrival can be coded in a lookup table. The expected improvement in performance of a wavefront sensor is derived under open-loop operations. For closed-loop performance estimates, we provide simulation results.

We model the signal from the sensor as a linear function of the input wavefront coefficients, with some noise caused by the Poisson statistics of the photon arrival process.

$$d = \Theta\alpha + n \quad (3)$$

where n is the noise due to the randomness of photon arrival. This is approximately Gaussian when the photon count is high, but for simplicity,

we continue to use the Gaussian approximation at low photon counts.

The wavefront estimate is given by

$$\hat{\alpha} = \Theta^+ d \quad (4)$$

where the inversion matrix Θ^+ is a Maximum-Likelihood estimate [4].

In our simulations, the wavefront sensor is operated in a closed control loop. For an incoming wavefront α_j at each time step j , cancelled with the previous wavefront estimate $\hat{\alpha}_{j-1}$ using the mirror, the residual wavefront entering the wavefront sensor is $\alpha_j - \hat{\alpha}_{j-1}$. The sensor signal d_j at each time step is thus given by

$$d_j = \Theta(\alpha_j - \hat{\alpha}_{j-1}) + n_j \quad (5)$$

with the inverse solution for the current wavefront estimate of

$$\hat{\alpha}_j = \hat{\alpha}_{j-1} + \gamma(\Theta^+ d_j) \quad (6)$$

where γ is a feedback loop gain factor used to adjust for the amount of noise in the data.

The optimal value for γ provides a trade-off between the wavefront estimate formed by previous photons and the wavefront estimate due to the current photon arrival. The optimal value of γ is determined empirically in the results presented here.

4 Simulations

The effects of atmospheric turbulence on wavefronts were simulated assuming that the random statistics of the atmosphere follow the Kolmogorov power law [5, 6]. The resulting static wavefront aberrations are simulated using the fractal generator of [7]. To simulate changing turbulence, we employ Taylor's frozen flow hypothesis, which models the evolution of aberrations over time using multiple layers of static turbulence moving across the telescope aperture. In our simulations, we consider a single layer of turbulence, representing the dominant layer of turbulence.

The parameters describing the simulation model is shown in figure 5. The diameter of the telescope $D = 1m$, and is sampled with 64×64 pixels ($n = 64$). The deformable mirror corrects for $m = 20$ Zernike modes. The simulations is run in discrete 0.5ms time steps.

The severity of turbulence is characterised by its coherence length $r_0 = 0.25m$. This reduces the

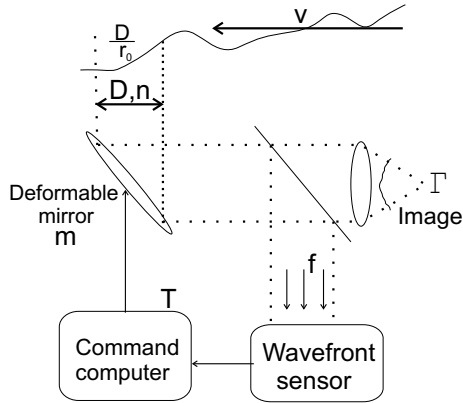


Figure 5: Simulation of the control loop in an adaptive optics system.

telescope resolution by a factor of 4. Its wind-speed, $v = 6.25 \text{ms}^{-1}$, was chosen so that together with the aperture sampling and duration of each time step, the turbulence (wavefront) at the aperture shifts by 1 pixel every 5 time steps.

f represents the mean photon count at the wavefront sensor at every time step. From the aperture diameter and time step duration, the telescope collects on average 1 photon in each time step from an 18-th magnitude guide star.

Γ , the Strehl ratio of the corrected image, is a measure of image quality. It compares the aberrated image peak with the peak of a perfect or diffraction-limited spot.

The relationship between the complex field at the focal plane and the aperture plane is described by the Fourier Transform [8]. Similarly, the images in the pyramid sensor are Fourier pairs of the complex field at the sub-divided focal plane. The intensity of the aperture images are given the squared magnitudes of the complex fields. We assume that the image detectors (for example CCD arrays) are capable of counting individual photons, and have no other instrumentation noise (no read noise or dark current noise). The process of photon arrival is assumed to follow Poisson statistics, with the probability distribution of the photons being given by the intensity distribution of the images at the focal plane.

For the control computer which calculates the wavefront and mirror actuation functions, a modal estimation and correction scheme, using the Zernike polynomials, is employed. The first twenty lowest order Zernike modes are used to describe the wavefront. This is sufficient to model the severity of turbulence.

The simulation made use of discrete time steps to simulate the control-loop operation. A more accurate model would use the statistics of the inter-arrival times between photons. However, this is not

expected to significantly affect the results for this simulation.

4.1 Simulation results

Simulations are performed to compare the operation of the single photon adaptive optics system with the conventional multi-photon system. Two simulations (using the parameters described in the previous section) are carried out for a period of 2.5 seconds (or 5000 time steps) using the same wavefront aberrations. At each time step, the wavefront residual is used to determine the image or probability distribution for the photon density.

The deformable mirror is updated to cancel the wavefront either at every time step (single photon system), or every 25 time steps (representing the longer integration time in a conventional wavefront sensor). The optimal value for γ (refer to equation (6)) is found to be 0.02 for both the single and multiple photon system.

As a controller of a dynamical system, the tracking error of the adaptive optics system provides a measure of its performance. The results from the simulations are shown in figure 6 and figure 7.

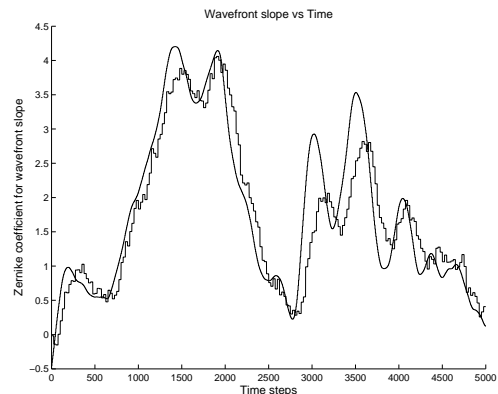


Figure 6: Wavefront slope tracking with a conventional wavefront sensor (25 photons per image frame, updated every 25 time steps, or 12.5ms).

For astronomical imaging, a more convenient measure is provided from the resultant image quality. This is conventionally measured with the Strehl ratio. In our simulations, the Strehl ratio is measured from the long term exposure images in the direct imaging channel. A comparison of the scaled cross-sections of the images at the telescope focal plane for a point-source object is shown in figure 8. The images are scaled so that the maximum height of a diffraction-limited spot is 1.

Before any wavefront correction was applied, the Strehl ratio of the turbulence degraded image is about 0.08. After closing the control loop, the image from both types of sensors show improvements

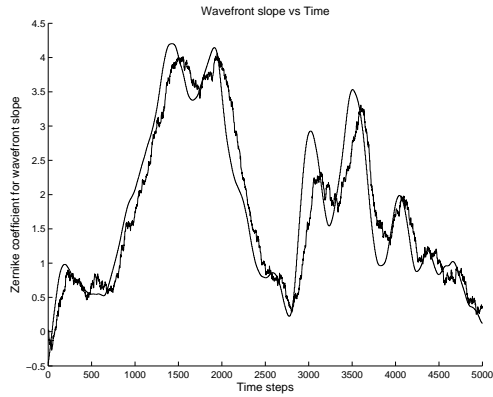


Figure 7: Wavefront slope tracking with a photon counting wavefront sensor (1 photon per image frame, updated every time step, 0.5ms).

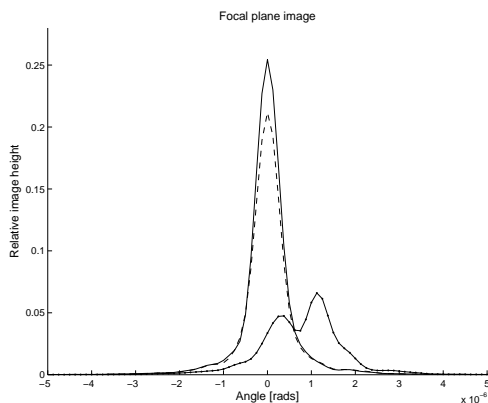


Figure 8: Images at the focal plane for an uncompensated open loop system (dotted line) and compensated systems with the conventional wavefront sensor (dashed line) and the photon counting wavefront sensor (solid line).

in their Strehl ratios. Using the conventional multiple photon wavefront sensor, the Strehl improved to 0.21, while using the single photon wavefront sensor, the Strehl ratio is further improved to 0.25.

The photon counting wavefront sensor has a performance improvement over a conventional wavefront sensor setup, due to a reduced control-loop lag time. For a fixed wind speed, this lag time is ultimately limited by the photon level, since the single photon wavefront sensor requires the information from several photons to form an acceptable wavefront estimate.

5 Conclusion

Although the simulation model employed here is sufficient for the purpose of demonstrating the single photon wavefront sensor, certain aspects of the simulation can be improved to provide a more complete model of the wavefront sensor. The noise model simplistically scales conditions under high

photon counts down to the single photon level, although the noise statistics are no longer Gaussian. For a more thorough treatment, the sensor signal noise needs to represent photon arrivals with shot noise statistics.

Under closed-loop conditions, a Kalman filter model can be used for wavefront estimation, with the temporal evolution of the wavefront coefficients expressed as a state space model. This allows us to analytically trade-off a-priori knowledge of wavefront statistics with sensor noise (compare with equation (5)).

In conclusion, single photon wavefront sensors have the potential to improve the performance of adaptive optics systems by reducing the control loop lag. Preliminary simulation results confirm an improvement in performance of such systems compared to conventional wavefront sensors.

6 Acknowledgements

This research is supported by a scholarship from the Keith Laugesen Memorial Trust.

References

- [1] R. K. Tyson, *Introduction to Adaptive Optics*. The International Society for Optical Engineering, 2000.
- [2] R. Ragazzoni, "Pupil plane wavefront sensing with an oscillating prism," *Journal of Modern Optics*, vol. 43, no. 2, pp. 289–293, 1996.
- [3] R. J. Noll, "Zernike polynomials and atmospheric turbulence," *Journal of the Optical Society of America*, vol. 66, no. 3, pp. 207–211, 1976.
- [4] S. M. Kay, *Fundamentals of Statistical Signal Processing: estimation theory*. Prentice Hall, 1993.
- [5] A. N. Kolmogorov, *The local structure of turbulence in incompressible viscous fluids for very large reynolds' numbers*. Wiley-Interscience, New York, 1961.
- [6] F. Roddier, "The effects of atmospheric turbulence in optical astronomy," *Progress in optics*, vol. 19, no. 5, pp. 281–376, 1981.
- [7] C. M. Harding, R. A. Johnston, and R. G. Lane, "Fast simulation of a kolmogorov phase screen," *Applied Optics*, vol. 38, no. 11, pp. 2161–2170, 1999.
- [8] J. Goodman, *Introduction to Fourier Optics*. McGraw-Hill, New York, 1996.